Journal of Marine Systems 239 (2023) 103844

Contents lists available at ScienceDirect

Journal of Marine Systems

journal homepage: www.elsevier.com/locate/jmarsys

Latitudinal variability and adaptation of phytoplankton in the Atlantic Ocean

R. Barlow [a,*], T. Lamont [b,a,c], J. Viljoen [d,f], R. Airs [e], R. Brewin [f,e], G. Tilstone [e], J. Aiken [e], E. Woodward [e], C. Harris [e]

[a] Bayworld Centre for Research & Education, Cape Town, South Africa
[b] Oceans & Coasts Research, Department of Forestry, Fisheries & Environment, Cape Town, South Africa
[c] Marine Research Institute & Department of Oceanography, University of Cape Town, South Africa
[d] Department of Earth Sciences, Stellenbosch University, Stellenbosch, South Africa
[e] Plymouth Marine Laboratory, Plymouth, United Kingdom
[f] Centre for Geography & Environmental Science, College of Life and Environmental Sciences, University of Exeter, Penryn, United Kingdom

ARTICLE INFO

Keywords:
Phytoplankton
Pigments
Hydrography
Atlantic Ocean

ABSTRACT

This study assessed the variability of a range of phytoplankton groups between repeat cruises over the mid-Atlantic Ocean (50°N-50°S), and demonstrated the important contribution of the pico-phytoplankton to the microalgal biomass in the oligotrophic tropical and sub-tropical regions. Pigment data from two meridional transects were analysed by quantitative chemotaxonomic analysis (CHEMTAX) to yield information concerning the composition of phytoplankton communities along the transects. Total chlorophyll *a* (TChla) in October–November 2012 (AMT22) and 2013 (AMT23) varied from 0.03 mg m^{-3} in the southern Sub-Tropical Gyre to 1.13 and 1.92 mg m^{-3} at 40°S and 42°S respectively. *Synechococcus* accounted for 35–50% and *Prochlorococcus* 30–35% of the TChla in oligotrophic surface waters on AMT22, while haptophytes dominated the temperate regions. *Prochlorococcus* was dominant (30–60%) on AMT23, with *Synechococcus* contributing 20–40% and haptophytes 10–20%, and it was noted that the dominance of *Prochlorococcus* occurred in water masses where the inorganic nitrate concentrations were extremely low (≤0.02 mmol m^{-3}). *Prochlorococcus* and haptophytes dominated the deep chlorophyll maximum (DCM) on AMT22, with the *Synechococcus* proportion being low, while *Prochlorococcus* was generally dominant on AMT23, although *Synechococcus* and haptophytes were also prominent. Photo-pigment indices indicated that chlorophyll *b* was mainly associated with *Prochlorococcus* but also related to prasinophytes. Chlorophyll *c* and photosynthetic carotenoids increased with an increase in the proportion of haptophytes and to a lesser extent with the proportion of diatoms and pelagophytes. *Prochlorococcus* and *Synechococcus* were the main contributors to the photoprotective carotenoids and relationships indicated that *Synechococcus* accounted for more of this pool in 2012, but the *Prochlorococcus* contribution was greater in 2013. Temperature, stratification, nutrients and light appeared to be the main hydrographic variables influencing phytoplankton composition along the transects.

1. Introduction

The Atlantic Ocean is an important basin in the global thermohaline circulation and is influenced by the mid-Atlantic Ridge and many islands. It also receives substantial freshwater inputs from several large river systems in the mid- to lower latitudes. While phytoplankton accounts for 50% of global primary production (Field et al., 1998), it is the biomass and community composition that influences the structure of marine food webs and are considered important indicators of how ecosystems respond to climate and anthropogenic change (Maloney and Field, 1991; Platt and Sathyendranath, 2008). It is in this context that the UK Atlantic Meridional Transect (AMT) programme was initiated to investigate the biogeochemical and ecological variability of plankton and to assess the effects on air-sea gas exchange and carbon cycling (Aiken et al., 2000; Robinson et al., 2006). The early AMT research cruises (1995–2000) tracked the eastern sectors of the North Atlantic and western boundary of the South Atlantic (Aiken et al., 2000; Robinson et al., 2006; Rees et al., 2017), but since 2000 the cruises have

* Corresponding author.
E-mail address: rgb.barlow@gmail.com (R. Barlow).

https://doi.org/10.1016/j.jmarsys.2022.103844
Received 30 May 2022; Received in revised form 22 September 2022; Accepted 28 November 2022
Available online 2 December 2022

focussed more towards the centre of the Atlantic basin to enable assessment of the Sub-Tropical Gyres and Tropical Equatorial Region (Robinson et al., 2006; Aiken et al., 2017; Rees et al., 2017).

Flow cytometry on AMT cruises revealed that the oligotrophic waters are usually dominated by the pico-prokaryotes *Prochlorococcus* and *Synechococcus* spp. and by pico-eukaryotes (Zubkov et al., 1998, 2000; Heywood et al., 2006; Tarran et al., 2006). Coccolithophore studies revealed a large number of taxa but species such as *Emiliania huxleyi* and *Gephyrocapsa ericsonii* are usually the most abundant in the lower euphotic zone in both temperate and tropical waters (Poulton et al., 2017). Pigment data has been produced routinely in support of bio-optical investigations, and also used to elucidate phytoplankton composition. Gibb et al. (2000) and Barlow et al. (2002) noted that elevated concentrations of divinyl chlorophyll *a* and zeaxanthin indicated prokaryote dominance in oligotrophic waters, complementing the flow cytometry results. Other pigment biomarkers signified nano-phytoplankton importance in mesotrophic zones and diatoms and dinoflagellates in temperate eutrophic regions (Gibb et al., 2000; Barlow et al., 2002, 2004; Poulton et al., 2006). An 8-year investigation (2003−2010) by Agirbas et al. (2015) demonstrated an increase in nano- and pico-phytoplankton during autumn in the northern gyre with no change in chlorophyll *a*, but both pico-phytoplankton and chlorophyll *a* increased in the southern gyre during the austral spring. Similarly, Tilstone et al. (2017) showed that pico-phytoplankton account for 60% of the primary production along the AMT transects in both boreal spring and autumn. Other European cruises demonstrated similar trans-Atlantic observations, where CHEMTAX analysis of pigments indicated *Prochlorococcus*, haptophytes and *Synechoccoccus* being the important groups in the tropical and subtropical Atlantic, and diatoms and haptophytes dominating the Patagonian continental shelf (Nunes et al., 2019). A meridional study by Bracher et al. (2020), employing bio-optics and diagnostic pigment analysis, observed *Prochlorococcus* and other cyanobacteria to be dominant in the sub-tropics and tropics, and haptophytes and diatoms in temperate regions.

The utility of CHEMTAX analysis of pigments to determine the contribution of phytoplankton groups to the total chlorophyll *a* (TChla) on Atlantic transects has been demonstrated by Nunes et al. (2019) (see above) and also for an AMT cruise in 1998 on the eastern boundary of the Atlantic (Barlow et al., 2016). The 1998 study indicated diatom dominance in the Benguela upwelling region, and diatoms and haptophytes in the Canary upwelling ecosystem and temperate NE Atlantic. *Prochlorococcus* was the most prominent group within the oligotrophic zone at 15.5°S-15°N, while haptophytes dominated between 21°N and 40°N (Barlow et al., 2016). In this communication, we use CHEMTAX data to assess phytoplankton community structure for AMT cruises in 2012 and 2013. These data sets were selected for examination because of interesting differences in hydrography and pigments along these transects. The objectives were to: 1) characterize and compare the community structure at the surface and the deep chlorophyll maximum (DCM) along the two transects; 2) determine whether *Prochlorococcus* or *Synechoccoccus* is more dominant in the gyres and equatorial regions; 3) assess the changing contributions of the chlorophylls and carotenoids to the total pigment pool.

2. Methods

The AMT22 cruise was undertaken on the RRS *James Cook* from the UK to Punta Arenas, Chile (10 October-24 November 2012), and the AMT23 cruise on the RRS *James Clark Ross* from the UK to the Falkland Islands (1 October-11 November 2013) (Fig. 1). Water column temperature, salinity and photosynthetically available radiation (PAR) were measured by CTD profiling at stations conducted at 0500 and 1300 GMT each day. The upper mixed layer (UML) was determined as the depth where the local change in density was ≥0.03 kg m^{-3} using potential density profiles and a threshold gradient criterion (Thomson and Fine, 2003). The depth of the deep chlorophyll maximum (DCM) was

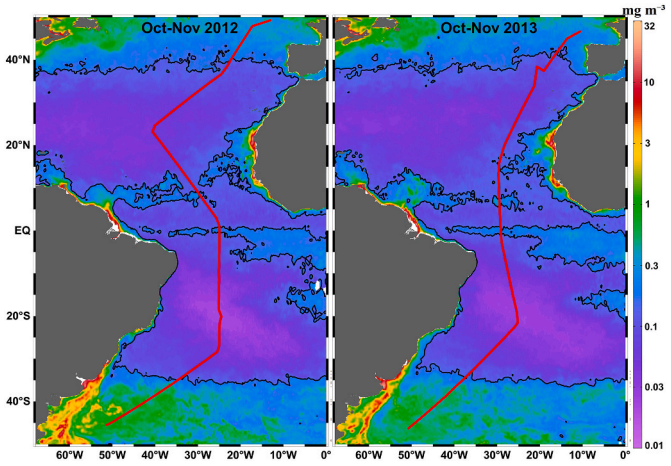

Fig. 1. AMT22 (October–November 2012) and AMT23 (October–November 2013) cruise tracks on MODIS Aqua TChla images. Black solid contours indicate 0.15 mg m^{-3} concentrations. (For interpretation of the references to colour in this figure legend, the reader is referred to the web version of this article.)

identified as the depth of maximum subsurface chlorophyll *a* observed from CTD fluorescence profiles, similar to previous studies (Cullen, 2015). The depth of the euphotic zone (Z_{eu}), defined where irradiance is 1% of the surface value, was estimated from the PAR profile according to Morel (1988). Following Brewin et al. (2012) and Behrenfeld et al. (2006), the density difference between the surface and 200 m was used as an indicator of stratification strength. Nutrient samples were collected at selected depths (2-300 m, AMT22; 2-400 m, AMT23) for onboard triplicate analysis by autoanalyser (Bran & Luebb) according to Woodward and Rees (2001), and for convenience nitrate and nitrite concentrations are summed and reported collectively as nitrate (NO3). Limits of detection were of the order of 0.02 mmol m^{-3}. Seawater samples for pigment analysis (1–4 L) were collected from the surface underway non-contaminated seawater supply (5 m) and from the DCM during CTD deployments, filtered through 25 mm GF/F filters that were frozen in liquid nitrogen, and then stored at -80 °C for analysis ashore.

Pigments were cold extracted on ice in 90% acetone for 3 h, aided by the use of ultrasonication, clarified by centrifugation and filtration, and analysed by HPLC (ThermoScientific Accela) using a Waters Symmetry C8 column (150 × 2.1 mm, 3.5 μm particle size, thermostatted at 25 °C) according to Zapata et al. (2000). Pigments were detected at 440 and 660 nm and identified by retention time and on-line diode array spectra. Monovinyl chlorophyll *a* standard was obtained from Sigma-Aldrich Ltd. and other pigment standards were purchased from the DHI Institute for Water and Environment, Denmark. Quality assurance protocols followed Van Heukelem and Hooker (2011). The method separates divinyl and monovinyl chlorophyll *a*, zeaxanthin and lutein, but does not resolve divinyl and monovinyl chlorophyll *b*. Therefore the total chlorophyll *b* data is divinyl plus monovinyl chlorophyll *b* (TChlb). Limits of detection were of the order of 0.001 mg m^{-3}.

To determine community composition, pigment data was analysed by CHEMTAX (Mackey et al., 1996; Wright, 2008) following Higgins et al. (2011), with chemotaxonomic groups being identified according to Jeffrey et al. (2011). An assumption made using CHEMTAX is that the pigment:chlorophyll *a* ratios are constant across all the samples within each analysis. Samples were therefore separated by depth and latitude, such that similar surface samples were analysed together within selected latitude ranges, and the DCM samples were analysed separately within comparable latitude ranges. Pigment starting ratios were obtained from Higgins et al. (2011) and the functional groups included the following: diatoms, dinoflagellates, cryptophytes, pelagophytes, haptophytes, prasinophytes-1, prasinophytes-3, *Synechococcus* spp. and *Prochlorococcus* spp. Although *Prochlorococcus* is also a cyanobacterium, the

distinct divinyl chlorophyll *a* signature allows *Prochlorococcus* to be distinguished from *Synechococcus* in the CHEMTAX analysis. To ease the presentation of the chemotaxonomic data, prasinophytes-1 and -3 were combined into a collective prasinophyte group. Starting ratios and optimised output ratios for each latitude range are presented in Table S1 in the supplementary data.

CHEMTAX outputs are the fraction of chlorophyll *a* attributed to each functional group specified in the matrix. The HPLC method separated monovinyl chlorophyll *a* allomer, monovinyl chlorophyll *a*, monovinyl chlorophyll *a* epimer and chlorophyllide *a*, and in CHEMTAX the sum of all 4 was used as the chlorophyll *a* concentration. Divinyl chlorophyll *a* was allocated entirely to *Prochlorococcus* spp. TChla was used as an index of phytoplankton biomass and is the sum of chlorophyll *a* plus divinyl chlorophyll *a*. The software may not discover the best global solution if it encounters local minima in the process. To circumvent this possibility, multiple starting points were used. Fifty-nine further pigment ratio tables were generated by multiplying each cell of the initial table by a randomly determined factor F, calculated as:

$$F = 1 + S \times (R - 0.5)$$

where S is a scaling factor of 0.7, and R is a random number between 0 and 1 generated using the Microsoft Excel RAND function (Wright et al., 2009). Each of the 60 ratio tables was used as the starting point for a CHEMTAX optimization, with the Higgins et al. (2011) ratios being used in the initial table. The solution with the smallest residual was used for the estimated phytoplankton group abundance.

Photo-pigment indices were derived to assess the changing contribution of chlorophylls and carotenoids to the total pigment pool (TPig). The chlorophylls were proportioned into TChla, TChlb and TChlc (chlorophyll c_1, chlorophyll c_2, chlorophyll c_3, Mg-2,4-divinyl pheoporphyrin a_5 monomethyl ester, chlorophyll c_2-monogalactosyldiacylglyceride ester [18:4/14:0], chlorophyll c_2-monogalactosyldiacylglyceride ester [14:0/14:0]). The carotenoids were partitioned into photosynthetic carotenoids (PSC) and photoprotective carotenoids (PPC) (Brunet et al., 2011; Johnsen et al., 2011), where PSC included peridinin, fucoxanthin, 19′-butanoyloxyfucoxanthin, 19′-hexanoyloxyfucoxanthin and prasinoxanthin. PPC consisted of neoxanthin, violaxanthin, diadinoxanthin, antheraxanthin, alloxanthin, diatoxanthin, zeaxanthin and $\beta\beta$-carotene.

3. Results

3.1. Hydrography

The 0.15 mg m^{-3} TChla contour is a suitable indicator to identify the boundaries of the gyres in the Atlantic as indicated by Aiken et al. (2000, 2009, 2017). The satellite images in Fig. 1 show that the 0.15 mg m^{-3} contours extended from approximately 40°-10°N in the North (N) Atlantic and from 5°-34°S in the South (S) Atlantic, indicating consistent limits of the northern and southern gyres in October–November 2012 and 2013. The Tropical Equatorial Region was therefore located between 10°N and 5°S (Fig. 1). The cruise tracks indicated that the AMT22 passage progressed to 40°W, closer to the centre of the N Atlantic gyre, then southeast towards the equator and south along 25°W through the centre of the S Atlantic gyre, progressing southwest from 28°S towards South America. The AMT23 passage did not advance to 40°W but tracked the eastern sector of the N Atlantic gyre, then headed south through the equatorial region to the centre of the S Atlantic gyre, thereafter progressing southwest towards South America. The MODIS Aqua images suggested that TChla levels were slightly more elevated north of 40°N and south of 35°S during October–November 2012 (AMT22) compared to October–November 2013 (AMT23). The images also appeared to indicate that TChla was slightly more elevated in the eastern tropical S Atlantic (0°-5°S, 0°-20°W) and the western tropical N Atlantic near the coastal regions of South America during AMT23 relative to AMT22.

Temperature variability at the surface along the AMT22 and AMT23 transects showed similar large-scale variations, with cool water (10-23 °C) in the temperate N and S Atlantic and warm water up to 28.7–28.9 °C in the tropics (Fig. 2a, c). Salinities of 35.5–35.6 were recorded at 47°-49°N, which increased to 37.5–37.7 in the N Atlantic gyre, and then declined to 34.7–34.8 in the equatorial zone. A similar pattern was observed in the S Atlantic with higher salinity in the gyre (Fig. 2a, c). Temperature at the DCM was lower overall on both transects but the pattern of change was similar to that observed at the surface (Fig. 3a, c). Salinity at the DCM also displayed elevated values in the gyres and was lower in the tropics and at higher latitudes, but the magnitude of difference between high and low salinities were considerably smaller than observed at the surface (Fig. 3a, c).

Surface nutrient concentrations were low for phosphate and nitrate along most of the AMT22 and AMT23 transects, and increased south of 30°S, particularly for nitrate (Fig. 2b, d). Surface silicate was elevated along both transects, 0.5–2.2 mmol m^{-3} on AMT22, but slightly lower at 0.4–1.8 mmol m^{-3} on AMT23 (Fig. 2b, d). Nutrients were higher overall at the DCM on both transects, although nitrate was highly variable between ≤0.02 and 8 mmol m^{-3} (Fig. 3b, d).

PAR varied considerably on AMT22 and AMT23, within the range of 80–1400 μE m^{-2} s^{-1} at the surface and 2–100 μE m^{-2} s^{-1} at the DCM (Fig. 4a, b). The UML depth was 10–60 m in the N Atlantic on AMT22, and 10–40 m in the S Atlantic, except at 8°S and 35°S where the UML reached 70 m (Fig. 4c). On AMT23, the UML was 10–40 m in the N Atlantic and 10–100 m in the S Atlantic (Fig. 4d). During AMT22, the strongest stratification (> 2 kg m^{-3}) was observed roughly between 20°S and 20°N, with maximum values observed at 8.2°N (Fig. 4c). Interestingly, this region of elevated stratification was shifted south during AMT23, with maximum stratification occurring at 7.4°S and values above 2 kg m^{-3} observed as far south as 30°S (Fig. 4d). These differences were likely due to interannual variations and shorter-term differences in physical forcing during the two cruises. Overall, stratification was weaker in the S Atlantic, while somewhat elevated values occurred in the N Atlantic during both cruises (Figs. 4c, d). The depth of Z_{eu} on AMT22 and AMT23 was 40–80 m in the temperate N and S Atlantic, deeper at 100–120 m in the northern gyre, shallowing to 60–100 m in the tropics, deepening again to 120–160 m in the southern gyre (Fig. 4c, d). The DCM tracked the pattern of Z_{eu} but was slightly shallower than Z_{eu} along most of the two transects, except in the gyres where the DCM was deeper at 100–130 m in the northern gyre and 140–170 m in the southern gyre (Fig. 4c, d).

3.2. Functional groups and pigments

Surface TChla on the AMT22 transect was 0.2–0.8 mg m^{-3} at 50-40°N and declined to 0.05–0.08 mg m^{-3} through 30-25°N, then increased within the tropics, with a peak at the equator of 0.53 mg m^{-3} (Fig. 5a). TChla declined into the S Atlantic to reach lowest concentrations of 0.03–0.04 mg m^{-3} at 17-24°S, increasing up to 1.13 mg m^{-3} further south within the higher latitudes (Fig. 5a). CHEMTAX revealed that haptophytes were dominant at 50°-45°N, and *Synechococcus* particularly, together with *Prochlorococcus*, dominated from 45°N to 33°S, except in the vicinity of 20°S where the haptophytes were elevated (Fig. 5b). Diatoms were generally very low but increased at 50°N, 9°N and 25°S, while prasinophytes contributed 10–25% along the entire transect (Fig. 5c). Haptophytes mainly dominated the community south of 33°S, but diatoms, dinoflagellates, pelagophytes and prasinophytes also made patchy contributions (Fig. 5b, c).

Underway surface sampling on AMT23 was less frequent, with a total of 75 samples compared to 223 samples collected on AMT22. Consequently, there was less detail in the TChla pattern, and therefore the TChla peak at the equator was unfortunately not clearly observed. The available data in Fig. 5d indicated declining TChla from 46°N to 34°N, low TChla (0.05 mg m^{-3}) between 34°N and 26°N, an increase from

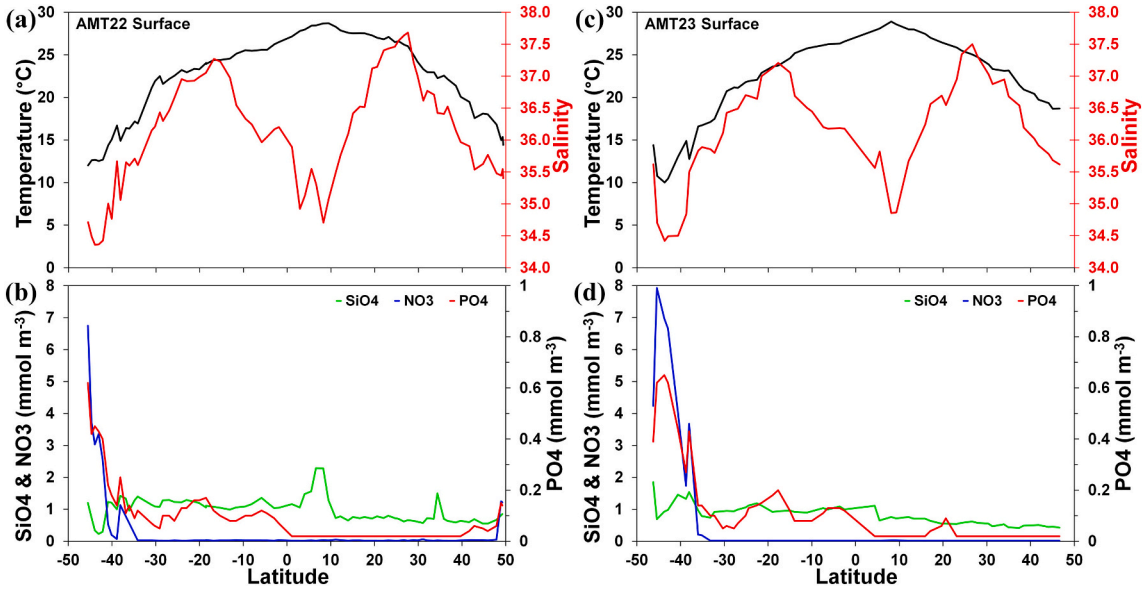

Fig. 2. Surface temperature (black), salinity (red), silicate (SiO4), phosphate (PO4) and nitrate (NO3) along the AMT22 (a, b) and AMT23 (c, d) transects. (For interpretation of the references to colour in this figure legend, the reader is referred to the web version of this article.)

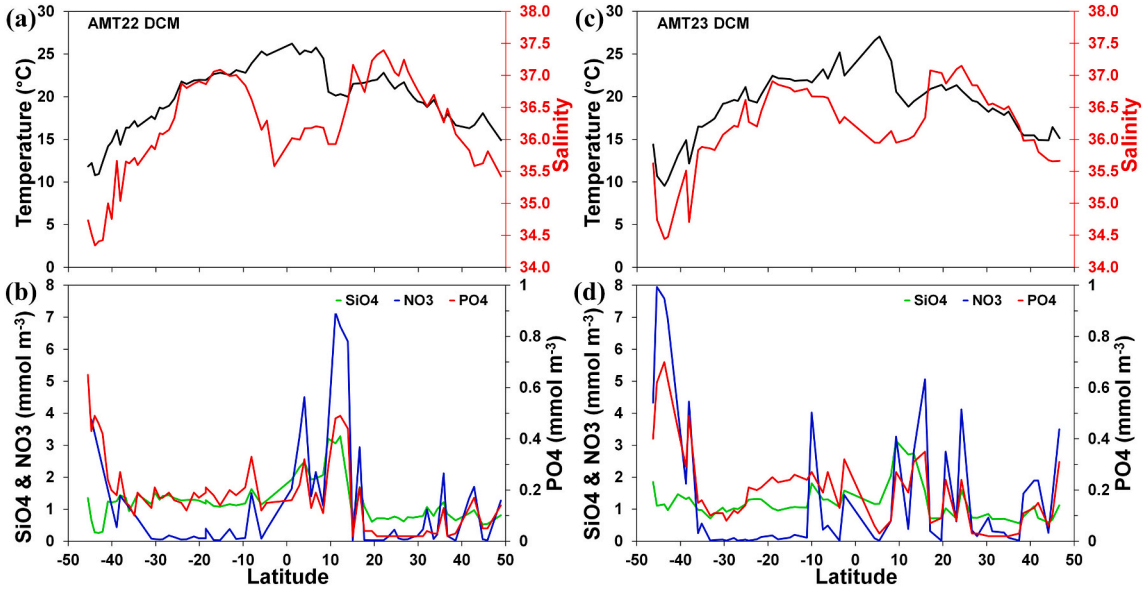

Fig. 3. Temperature (black), salinity (red), silicate (SiO4), phosphate (PO4) and nitrate (NO3) at the deep chlorophyll maximum (DCM) along the AMT22 (a, b) and AMT23 (c, d) transects. (For interpretation of the references to colour in this figure legend, the reader is referred to the web version of this article.)

26°N to 8°S, lowest TChla of 0.03 mg m^{-3} at 15-22°S, and increasing concentrations thereafter with a maximum of 1.92 mg m^{-3} at 42°S. *Prochlorococcus* dominated the community from 47°N to 33°S, with *Synechococcus* also significant and contributing a greater proportion at 15-13°N, while haptophytes and prasinophytes were generally of secondary importance (Fig. 5e, f). The proportions of diatoms, haptophytes and prasinophytes increased substantially from 33°S to 46°S, and there were also increases in dinoflagellates, pelagophytes and cryptophytes (Fig. 5e, f).

TChla was greater at the DCM than at the surface and varied with the changes in DCM depth, where TChla was higher in the temperate N and S Atlantic and the equatorial zone, but lower in the two gyres (Fig. 6a, d). *Prochlorococcus* and haptophytes were the dominant groups from 49°-30°S on AMT22, with the pelagophyte proportion also notable, but south of 30°S there was a sharp decline in *Prochlorococcus* and a lower proportion of haptophytes, while there were increased contributions by all the other groups (Fig. 6b, c). For AMT23, *Prochlorococcus* tended to be dominant between 47°N and 30°S, together with *Synechococcus* and haptophytes, and prasinophytes and pelagophytes were also prominent (Fig. 6e, f). Haptophytes dominated at 12-9°N and were also dominant at 30-46°S (Fig. 6e).

Photopigment indices revealed TChla ratios of 0.4–0.6 at the surface on the AMT22 transect, with PPC being more elevated than PSC between 42°N and 33°S, while PSC was greater at 49°-42°N and 33°-46°S, and TChlb and TChlc were low overall (Fig. 7a). The pattern at the DCM showed lower TChla indices of 0.4, with PSC being greater than PPC along the transect, and elevated TChlb between 34°N and 30°S (Fig. 7b). TChla indices at the surface on AMT23 were 0.3–0.5, while PPC was considerably elevated, exceeding TChla between 8°S and 15°S, but then decreased with the increase in PSC at 30°-46°S (Fig. 7c). The TChla

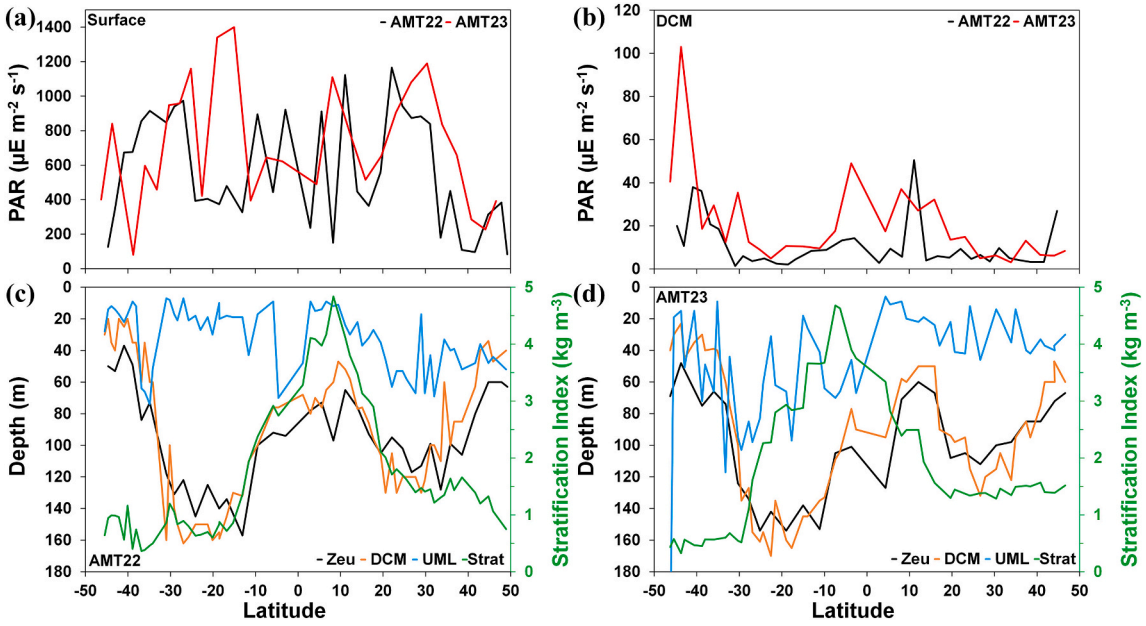

Fig. 4. Photosynthetically available radiation (PAR) at the surface (a) and DCM (b) for stations at 1300 GMT, and depths of the euphotic zone (Z_{eu}), DCM and upper mixed layer (UML), and stratification index (Strat) (c, d) along the AMT22 and AMT23 transects. (μE m^{-2} s^{-1} = μEinsteins m^{-2} s^{-1}).

index was 0.4–0.5 at the DCM, while PSC and TChlb varied approximately concurrently on most of the transect to 30°S, where PSC increased significantly towards 46°S (Fig. 7d).

3.3. Regression analysis

Linear regressions were performed between hydrographic variables and the proportion of each phytoplankton group for total cruise data sets, independently for the surface and for the DCM. This was specifically done to determine if differences existed for surface and DCM relationships between phytoplankton groups and environmental parameters. Regressions indicated that temperature, nutrients and stratification were the variables that had a statistically significant influence on phytoplankton group distribution. Negative slopes were noted for the regression of eukaryotes versus temperature, indicating decreases in the proportion of these groups as temperature increased. In contrast, positive slopes for *Synechococcus* and *Prochlorococcus* reflected increased proportions with increasing temperature (Table 1). Positive slopes were mostly observed for eukaryotes versus nutrients and negative slopes for *Synechococcus* and *Prochlorococcus* (Tables 2 and 3).

Regressions between temperature and groups indicated that R^2 and the F-statistic were significant for most of the group proportions (Table 1). Highest statistical significance at the surface was noted for haptophytes, pelagophytes, *Synechococcus* and *Prochlorococcus* for AMT22, and diatoms, haptophytes, cryptophytes, *Synechococcus* and *Prochlorococcus* for AMT23. For the DCM, strongest statistics were for diatoms, prasinophytes and *Prochlorococcus* for AMT22, and diatoms, haptophytes, cryptophytes and *Prochlorococcus* for AMT23.

Regressions between nutrients and group proportions (Tables 2 and 3) yielded strongest statistics for haptophytes, pelagophytes, *Synechococcus* and *Prochlorococcus* with both nitrate and phosphate for the AMT 22 surface, and diatoms, cryptophytes, *Synechococcus* and *Prochlorococcus* for AMT 23 surface. The R^2 and F-statistics for nutrient regressions were low overall for the AMT 22 DCM, but these statistics were strongest for diatoms, haptophytes, cryptophytes, *Synechococcus* and *Prochlorococcus* for the DCM on AMT23.

Stratification and group proportion regressions revealed low R^2 and the F-statistic for the DCM for both transects, but stronger relationships were observed for the surface (Table 4). Strongest statistics were noted for *Synechococcus*, *Prochlorococcus* and pelagophytes on AMT22, and *Synechococcus*, prasinophytes, pelagophytes and *Prochlorococcus* for AMT23 (Table 4).

4. Discussion

The temperature and salinity conditions at the surface were similar on the AMT22 and AMT23 transects, where maximum temperatures and low salinities were observed at 10-8°N (Fig. 2). In the N Atlantic, salinities increased from the higher latitudes to a maximum in the northern gyre, probably due to evaporation exceeding precipitation resulting in generally elevated salinity in the central region of the gyre. Salinities then decreased to a low level in the equatorial region where precipitation exceeded evaporation, resulting in overall lower salinities due to freshwater input from the rain and possibly the Amazon River plume (Aiken et al., 2000). A similar pattern is seen in the S Atlantic, with elevated salinity in the southern gyre at 16-18°S, then decreasing again at the higher southern latitudes where upwelling processes and eddy activity were likely towards the Patagonian shelf of S America (Fig. 2).

Nutrient levels suggested that silicate may possibly not be limiting at the surface or at the DCM on both transects compared to nitrate and phosphate, but Egge and Aksnes (1992) report that diatom growth is limited if silicate levels are below 2 mmol m^3. Silicate was mostly <2 mmol m^3 on both AMT22 and AMT 23 (Figs. 2 and 3) and the diatom proportion was very low, except at latitudes >35°S where diatoms increased (Figs. 5 and 6). This increase may reflect the greater availability of nitrate and phosphate as the diatoms may have taken up sufficient silicate at these latitudes. Nitrate was very low in the surface layer from 49°N to 33°S, where concentrations were ≤ 0.02–0.07 mmol m^{-3} in the oligotrophic waters on AMT22, while AMT23 levels were ≤ 0.02 mmol m^{-3} to 33°S and ≤ 0.02–0.07 mmol m^{-3} at 33°-37°S (Fig. 2d). These concentrations are at, or very close to, the detection limit for the analysis and may actually have been below these levels. Although there was a greater availability of nitrate at the DCM during both cruises, the range in concentration was quite considerable (Figs. 2 and 3).

Irradiance measurements indicated that PAR was highly variable at the surface and DCM on both transects, with a tendency for PAR to be

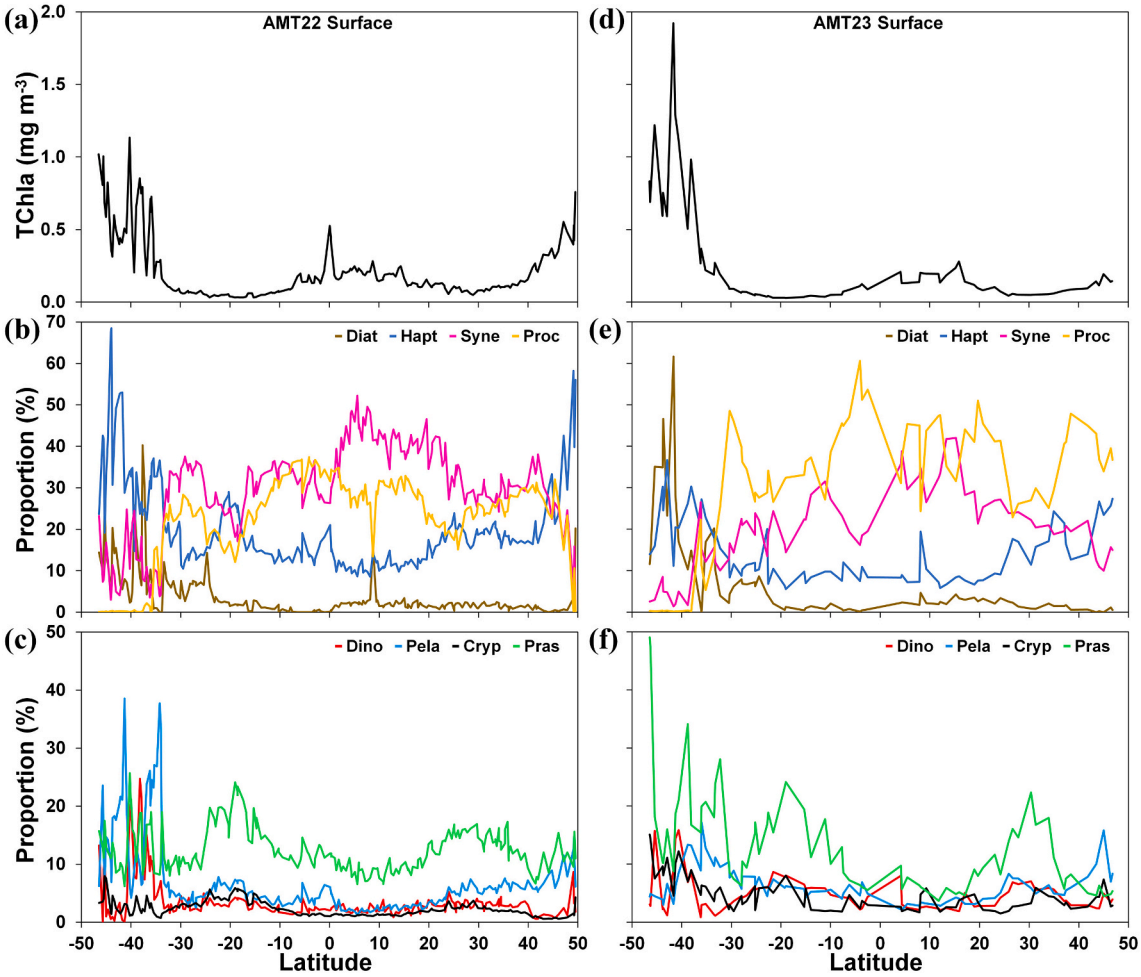

Fig. 5. Total chlorophyll *a* (TChla) and proportional contributions of phytoplankton groups at the surface along the AMT22 (a, b, c) and AMT23 (d, e, f) transects. Diat-diatoms (brown); Hapt-haptophytes (blue); Syne-*Synechococcus* (pink); Proc-*Prochlorococcus* (gold); Dino-dinoflagellates (red); Pela-pelagophytes (light blue); Cryp-cryptophytes (black); Pras-prasinophytetes (green). (For interpretation of the references to colour in this figure legend, the reader is referred to the web version of this article.)

slightly higher on AMT23 compared to AMT22 (Fig. 4a, b). PAR also appeared to be higher in the southern hemisphere compared to the northern hemisphere and this was most likely due to increased irradiance in austral spring in the S Atlantic as opposed to boreal autumn in the N Atlantic. On both transects, the depth of Z_{eu} was shallower in the temperate N and S Atlantic and through the equatorial zone, but deeper in the gyres (Fig. 4c, d). Z_{eu} was deeper in the southern gyre compared to the northern gyre and this may also be due to the higher PAR levels during the austral spring. Although the DCM generally followed the pattern of Z_{eu} but located slightly shallower, it is interesting that the DCM was 10–40 m deeper than Z_{eu} in the two gyres (Fig. 4c, d). The UML was estimated from density profiles and may be considered as the uppermost layer of uniform density that is driven by diurnal fluctuations in sea surface temperature and the exchange of heat with the overlying atmosphere (Thompson and Fine, 2003), but can also be influenced by changes in vertical mixing driven by variations in wind. Overall, the UML was generally deeper in the N Atlantic than the S Atlantic during AMT22, while on AMT23 the UML was deeper in the S Atlantic than the N Atlantic (Fig. 4c, d). The N Atlantic was somewhat more stratified than the S Atlantic, with substantially stronger stratification observed in the equatorial regions, during both cruises (Fig. 4c, d). This large-scale pattern is in agreement with the spatial patterns described in other global studies using more advanced stratification indices (Li et al., 2020, among others). Further details of the variability in environmental conditions in the North and South Atlantic over two decades of AMT has been synthesized and discussed by Aiken et al. (2017).

The changes in TChla on both transects indicated more elevated levels at the surface in temperate waters north of 40°N and south of 34°S, low concentrations in the two gyres, and some increase in the tropical region (Fig. 5). More frequent underway sampling during AMT22 enabled a peak in TChla to be observed at the equator, but this was not evident on AMT23 due to longer sampling intervals. Thus the limited surface data for AMT23 compared to AMT22 compromised the detail in latitudinal variability for AMT23. TChla was highly variable and patchy in the temperate southern waters, complementing the images in Fig. 1, and probably reflected eddy activity and upwelling in this region (Garzoli and Garraffo, 1989; Smyth et al., 2017). The weak stratification and much shallower Zeu and DCM depth (Fig. 4c) are consistent with the uplift and mixing driven by these processes. The patterns at the DCM were different and there was a tendency for TChla to be more elevated where the DCM was shallower, and lower at the deeper DCM's in the two gyres (Fig. 6). This pattern was more pronounced for AMT23 than for AMT22 and it is likely that the TChla was regulated by the depth of the nitracline and/or the nitracline gradient, since the DCM variation followed the pattern of nitrate concentration (Figs. 3 and 4). Irradiance likely also had an influence on TChla since light levels would be higher at shallow DCM's and lower deeper in the water column as demonstrated in Fig. 4b and also observed by Barlow et al. (2010) and Mitchell et al. (1991).

Stratification curbs the turbulence within the upper mixed layer

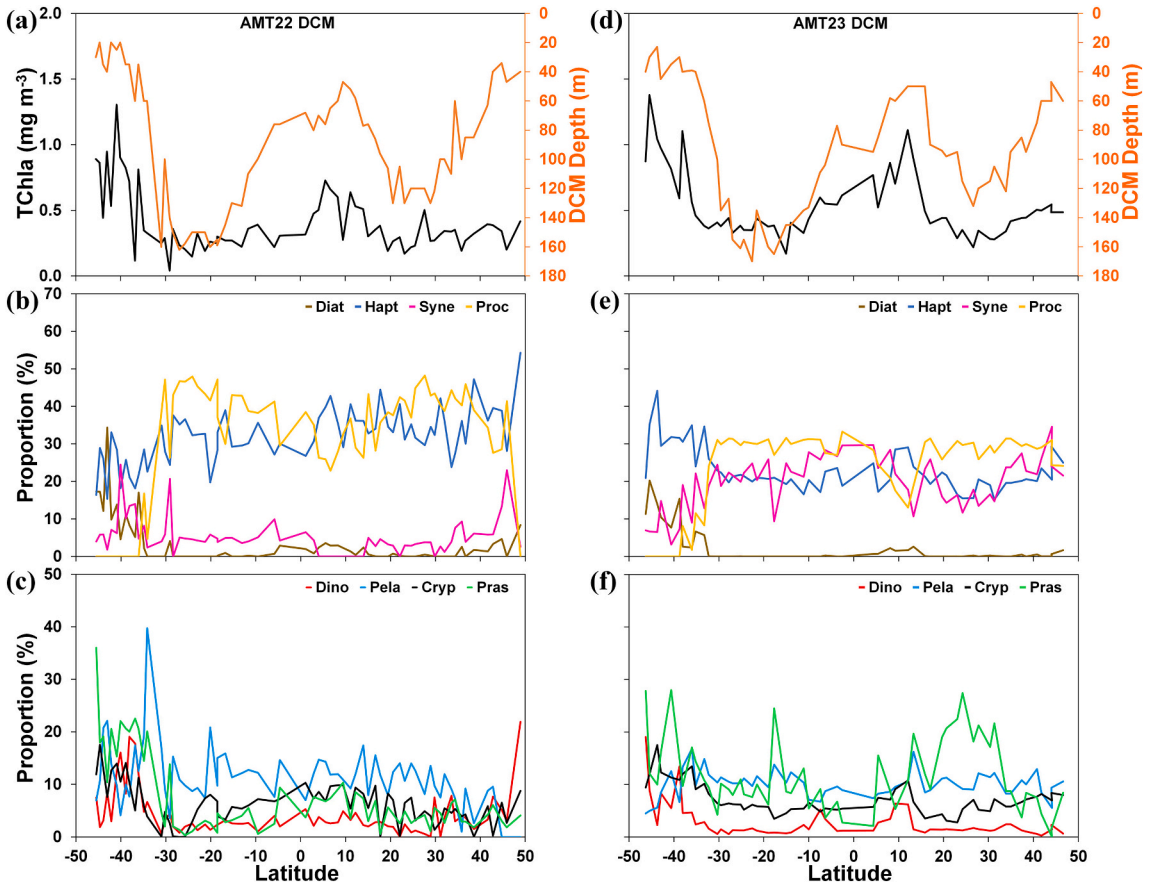

Fig. 6. Total chlorophyll *a* (TChla) and proportional contributions of phytoplankton groups at the deep chlorophyll maximum (DCM) along the AMT22 (a, b, c) and AMT23 (d, e, f) transects. The depth of the DCM (orange) is indicated in (a) and (d). Diat-diatoms (brown); Hapt-haptophytes (blue); Syne-*Synechococcus* (pink); Proc-*Prochlorococcus* (gold); Dino-dinoflagellates (red); Pela-pelagophytes (light blue); Cryp-cryptophytes (black); Pras-prasinophytetes (green). (For interpretation of the references to colour in this figure legend, the reader is referred to the web version of this article.)

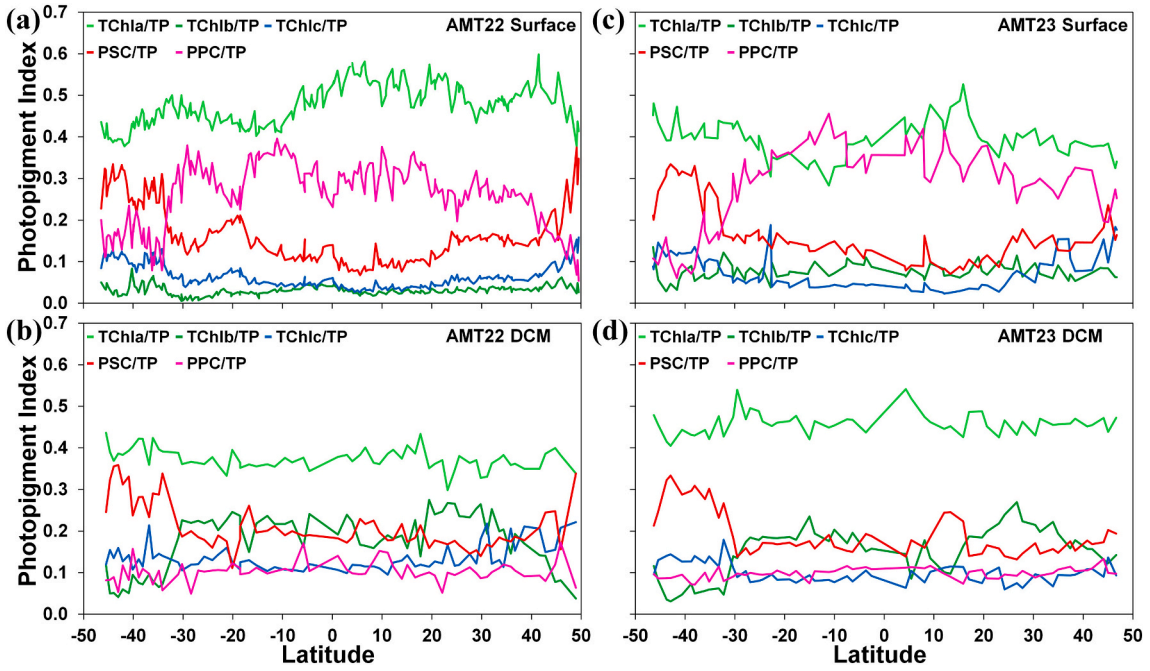

Fig. 7. Photo-pigment indices at the surface and deep chlorophyll maximum (DCM) along the AMT22 (a, b) and AMT23 (c, d) transects. TChla = total chlorophyll a; TChlb = total chlorophyll *b*; TChlc = total chlorophyll *c*; PSC = photosynthetic carotenoids; PPC = photoprotective carotenoids.

Table 1
Linear regression analysis between temperature and phytoplankton group proportions. Grey shading indicates significant relationships ($p < 0.05$). Diat-diatoms; Dino-dinoflagellates; Hapt-haptophytes; Pela-pelagophytes; Cryp-cryptophytes; Pras-prasinophytes; Syne-Synechococcus; Proc-Prochlorococcus.

	Group Proportion	Regression equation	R^2	F statistic	p value
AMT22 Surface					
Temperature	**Diat**	y = -0.462x + 13.585	0.259	6.648	0.018
	Dino	y = -0.287x + 10.091	0.142	3.151	0.092
	Hapt	y = -1.865x + 62.817	0.712	46.945	<0.001
	Pela	y = -1.132x + 33.350	0.691	42.500	<0.001
	Cryp	y = -0.027x + 3.048	0.009	0.165	0.690
	Pras	y = -0.011x + 13.156	0.000	0.004	0.951
	Syne	y = 2.069x − 18.538	0.760	60.302	<0.001
	Proc	y = 1.714x − 17.509	0.490	18.268	<0.001
AMT23 Surface					
Temperature	**Diat**	y = -1.318x + 34.850	0.542	50.945	<0.001
	Dino	y = -0.209x + 9.512	0.125	6.139	0.017
	Hapt	y = -1.048x + 37.560	0.520	46.648	<0.001
	Pela	y = -0.371x + 14.859	0.302	18.636	<0.001
	Cryp	y = -0.354x + 12.429	0.531	48.662	<0.001
	Pras	y = -0.650x + 27.080	0.230	12.859	0.001
	Syne	y = 1.623x − 15.288	0.776	148.606	<0.001
	Proc	y = 2.327x − 21.003	0.600	64.403	<0.001
AMT22 DCM					
Temperature	**Diat**	y = -1.031x + 23.290	0.425	47.305	<0.001
	Dino	y = -0.566x + 15.426	0.224	18.469	0.001
	Hapt	y = 0.600x + 20.212	0.095	6.742	0.012
	Pela	y = 0.004x + 11.220	0.000	0.000	0.986
	Cryp	y = -0.250x + 11.185	0.059	4.023	0.049
	Pras	y = -1.132x + 29.552	0.347	33.955	<0.001
	Syne	y = -0.445x + 13.890	0.111	8.015	0.006
	Proc	y = 2.820x − 24.775	0.416	45.598	<0.001
AMT23 DCM					
Temperature	**Diat**	y = -0.735x + 15.887	0.411	36.303	<0.001
	Dino	y = -0.336x + 9.074	0.150	9.153	0.004
	Hapt	y = -0.914x + 40.249	0.368	30.305	<0.001
	Pela	y = 0.043x + 9.208	0.004	0.220	0.641
	Cryp	y = -0.543x + 17.384	0.531	58.805	<0.001
	Pras	y = -0.184x + 15.128	0.010	0.543	0.464
	Syne	y = 0.867x + 3.494	0.223	14.941	<0.001
	Proc	y = 1.801x − 10.424	0.413	36.527	<0.001

leading to reduced UML depths, which in turn lessens the light limitation experienced by phytoplankton, but will simultaneously restrict the input of nutrients into the surface layers (Behrenfeld et al., 2006; Mahadevan et al., 2012). As such, stratification is also expected to influence the TChla distributions, with stronger stratification typically associated with lower TChla, and weaker stratification related to higher TChla values (Behrenfeld et al., 2006). Thus, much lower TChla was expected in association with the strong stratification in the equatorial region, with the opposite pattern occurring in the gyres where stratification was overall weaker. However, the opposite pattern was observed (Fig. 4c, d; Fig. 5a, d, and Fig. 6a, d). Thus, it appears that light and nutrient availability played a stronger role than stratification in influencing the observed TChla patterns. Other Atlantic meridional studies observed slightly higher TChla in the two gyres, where Nunes et al. (2019) reported TChla of 0.06 mg m^{-3} in the southern gyre and 0.20 mg m^{-3} in the northern gyre (October–November 2014), while Bracher et al. (2020) determined 0.15 and 0.18 mg m^{-3} respectively in May–June 2018. These differences from AMT observations could possibly reflect the phytoplankton response to subtle differences in environmental conditions during each cruise depending on the season, or the location and timing of the AMT track.

There were distinct differences in community structure between the two transects. *Synechococcus* was generally the dominant group (35–50%) in oligotrophic surface waters on AMT22, although *Prochlorococcus* was also prominent (30–35%), while haptophytes dominated temperate regions (Fig. 5). In contrast, *Prochlorococcus* was more dominant (30–60%) on AMT23, with *Synechococcus* being of secondary importance (20–40%), and the haptophyte proportion was lower (10–20%). The pattern at the DCM was different, where *Prochlorococcus* and haptophytes dominated (30–45%) on AMT22 and *Synechococcus* was low (Fig. 6). For AMT23, *Prochlorococcus* was generally dominant (30%), although *Synechococcus* was also prominent (20–30%) together with haptophytes (20%) (Fig. 6). There was an exception at 10°N, however, where TChla was elevated, coincident with a shallow DCM, and the haptophyte proportion was twice that of *Prochlorococcus* and *Synechococcus* (Fig. 6e). These observations are comparable with Nunes et al. (2019) who reported that *Prochlorococcus* (30–40%), haptophytes (25–30%) and *Synechococcus* (15–25%) were the most important phytoplankton groups in the tropical and subtropical Atlantic during boreal autumn and austral spring. Similarly, Bracher et al. (2020) also determined that *Prochlorococcus* (30–40%), cyanobacteria (30%, presumably *Synechococcus*) and haptophytes (10–15%) were the main

Table 2
Linear regression analysis between nitrate and phytoplankton group proportions. Grey shading indicates significant relationships ($p < 0.05$). Diat-diatoms; Dino-dinoflagellates; Hapt-haptophytes; Pela-pelagophytes; Cryp-cryptophytes; Pras-prasinophytes; Syne-Synechococcus; Proc-Prochlorococcus.

	Group Proportion	Regression equation	R^2	F statistic	p value
AMT22 Surface					
Nitrate	Diat	y = 1.610x + 2.484	0.052	0.935	0.347
	Dino	y = -0.369x + 2.688	0.020	0.344	0.565
	Hapt	y = 13.800x + 17.828	0.579	23.425	<0.001
	Pela	y = 6.434x + 5.276	0.699	39.389	<0.001
	Cryp	y = -0.324x + 2.339	0.020	0.354	0.560
	Pras	y = -0.977x + 12.629	0.031	0.541	0.472
	Syne	y = -10.452x + 31.906	0.423	12.454	0.003
	Proc	y = -9.723x + 24.850	0.333	8.480	0.010
AMT23 Surface					
Nitrate	Diat	y = 4.353x + 2.544	0.832	213.599	<0.001
	Dino	y = 0.630x + 4.429	0.160	8.177	0.007
	Hapt	y = 2.037x + 12.899	0.277	16.465	<0.001
	Pela	y = 0.020x + 6.636	0.000	0.005	0.942
	Cryp	y = 0.857x + 3.981	0.438	33.563	<0.001
	Pras	y = 0.817x + 12.093	0.051	2.318	0.135
	Syne	y = -3.023x + 22.814	0.379	26.212	<0.001
	Proc	y = -5.692x + 34.604	0.505	43.871	<0.001
AMT22 DCM					
Nitrate	Diat	y = 0.471x + 1.124	0.069	3.985	0.051
	Dino	y = 0.233x + 3.312	0.011	0.615	0.436
	Hapt	y = 0.583x + 32.868	0.025	1.392	0.243
	Pela	y = 0.308x + 10.552	0.008	0.458	0.501
	Cryp	y = 0.883x + 4.759	0.179	11.755	0.001
	Pras	y = 0.780x + 4.657	0.079	4.654	0.035
	Syne	y = -0.802x + 5.505	0.095	5.640	0.021
	Proc	y = -2.456x + 37.223	0.116	7.102	0.010
AMT23 DCM					
Nitrate	Diat	y = 1.435x − 0.033	0.459	44.133	<0.001
	Dino	y = 0.668x + 1.779	0.174	10.927	0.002
	Hapt	y = 1.439x + 20.952	0.267	18.978	<0.001
	Pela	y = -0.398x + 10.588	0.107	6.238	0.016
	Cryp	y = 0.761x + 6.047	0.305	22.843	<0.001
	Pras	y = 0.723x + 10.618	0.047	2.556	0.116
	Syne	y = -1.541x + 22.067	0.206	13.514	0.001
	Proc	y = -3.088x + 27.983	0.355	28.628	<0.001

groups in the northern and southern gyres, and the tropical region, in the boreal spring and austral autumn. A further interesting comparison can be made with the eastern boundary of the Atlantic where *Prochlorococcus* (40%) and haptophytes (25%) were the major groups in oligotrophic waters between 15°N and 16°S, while haptophytes (40%) and *Prochlorococcus* (15%) plus diatoms (15%) were dominant in a northern oligotrophic region at 40-21°N (Barlow et al., 2016).

The variability in the composition of pigments along the AMT22 and AMT23 transects, as demonstrated by the photo-pigment indices in Fig. 7, was associated with the changes in phytoplankton groups. TChla was the dominant pigment pool overall, with PPC's being elevated at the surface in the oligotrophic gyres and equatorial region, and PSC at the higher latitudes, while TChlb was greater at the DCM than in the surface layer. TChlb was associated with both *Prochlorococcus* and prasinophytes, and the steeper slopes for *Prochlorococcus* in Figs. 8a and 9a suggest that the contribution of divinyl chlorophyll *b* to the TChlb pool by *Prochlorococcus* in surface waters was greater than monovinyl chlorophyll *b* by prasinophytes. Although the TChlc index was low compared to PSC (Fig. 7a, c), the relationships in Figs. 8 (b, c) and 9 (b, c) indicate that the increases in both TChlc and PSC were associated mainly with an increase in the proportion of haptophytes, and to a lesser extent to the proportion of diatoms and pelagophytes, particularly for AMT22. The major contributors to PPC were *Prochlorococcus* and *Synechococcus* and the steeper slope in Fig. 8d suggests that *Synechococcus* accounted for more of the PPC pool in 2012 (AMT22). In contrast, the slopes in Fig. 9d indicate that the contribution to PPC by *Prochlorococcus* was greater than *Synechococcus* in 2013 (AMT23). Barlow et al. (2016) also determined that an increase in PSC was associated with haptophytes and increases in PPC were due to *Prochlorococcus* on the eastern boundary of the Atlantic. The proportion of PPC at the surface in the gyres and tropical region can be up to 40–45% of total pigments (Figs. 8d and 9d), although the less data available for AMT23 compared to AMT22 probably has an influence on the confidence of these relationships. Nevertheless, the dominance of PPC is evident and Smyth et al. (2017) estimated that the ratio of PPC to photosynthetic pigments (TChla, TChlb, TChlc, PSC) can be up to 1:1 in these low latitudes. Elevated PPC can have the effect of lowering the measurement of maximum quantum yields of photosynthesis and it is suggested that this can be corrected for by estimating the photosynthetically active absorption coefficients of PSC and chlorophylls *a*, *b* and *c* by the spectral reconstruction technique (Johnsen et al., 2011).

The interesting difference between cruises in the dominance of either

Table 3
Linear regression analysis between phosphate and phytoplankton group proportions. Grey shading indicates significant relationships ($p < 0.05$). Diat-diatoms; Dino-dinoflagellates; Hapt-haptophytes; Pela-pelagophytes; Cryp-cryptophytes; Pras-prasinophytes; Syne-Synechococcus; Proc-Prochlorococcus.

	Group Proportion	Regression equation	R^2	F statistic	p value
AMT22 Surface					
Phosphate	Diat	y = 19.195x + 1.380	0.177	3.649	0.073
	Dino	y = 0.545x + 2.587	0.001	0.018	0.896
	Hapt	y = 84.601x + 14.089	0.520	18.396	<0.001
	Pela	y = 39.616x + 3.520	0.632	29.200	<0.001
	Cryp	y = 0.296x + 2.264	0.000	0.007	0.935
	Pras	y = -6.226x + 12.910	0.030	0.524	0.479
	Syne	y = -78.524x + 35.772	0.570	22.494	<0.001
	Proc	y = -59.502x + 27.477	0.297	7.198	0.016
AMT23 Surface					
Phosphate	Diat	y = 49.031x − 0.248	0.786	157.798	<0.001
	Dino	y = 7.803x + 3.941	0.182	9.575	0.003
	Hapt	y = 22.955x + 11.592	0.262	15.235	<0.001
	Pela	y = 2.381x + 6.363	0.013	0.569	0.455
	Cryp	y = 11.207x + 3.244	0.558	54.269	<0.001
	Pras	y = 15.124x + 10.856	0.130	6.447	0.015
	Syne	y = -39.255x + 25.380	0.475	38.951	<0.001
	Proc	y = -69.245x + 38.872	0.556	53.874	<0.001
AMT22 DCM					
Phosphate	Diat	y = 9.660x + 0.199	0.134	8.362	0.006
	Dino	y = 4.424x + 2.906	0.019	1.036	0.313
	Hapt	y = -2.640x + 33.871	0.002	0.129	0.721
	Pela	y = 10.539x + 9.326	0.046	2.576	0.114
	Cryp	y = 13.546x + 3.696	0.195	13.085	0.001
	Pras	y = 15.555x + 3.190	0.146	9.238	0.004
	Syne	y = -5.831x + 5.518	0.023	1.280	0.263
	Proc	y = -45.251x + 41.294	0.183	12.083	0.001
AMT23 DCM					
Phosphate	Diat	y = 19.032x − 1.738	0.470	46.088	<0.001
	Dino	y = 9.313x + 0.896	0.196	12.679	0.001
	Hapt	y = 21.295x + 18.803	0.341	26.873	<0.001
	Pela	y = -3.425x + 10.693	0.046	2.514	0.119
	Cryp	y = 10.135x + 5.135	0.315	23.880	<0.001
	Pras	y = 6.365x + 10.399	0.021	1.121	0.295
	Syne	y = -19.713x + 23.754	0.196	12.705	0.001
	Proc	y = -43.004x + 32.058	0.401	34.753	<0.001

of the prokaryotes is probably related to the competition between *Synechococcus* and *Prochlorococcus* for resources in the oligotrophic gyres. *Synechococcus* appears to prefer temperatures >15 °C, sufficient light and detectable inorganic nutrients (Smyth et al., 2017), while *Prochlorococcus* can exploit conditions of both high and low light (Partensky et al., 1999), warm and cool temperatures, and very low inorganic nutrients (Smyth et al., 2017). Thus, differences in distribution of *Synechococcus* and *Prochlorococcus* can reveal important trophic distinctions among marine ecosystems (Bracher et al., 2020; Zubkov et al., 1998, 2000). Some evidence for these differences with regard to nutrients is illustrated in Fig. 10, where nitrate was ≤0.02–0.07 mmol m^{-3} in oligotrophic surface waters on AMT22 and *Synechococcus* tended to be a higher proportion of TChla than *Prochlorococcus*. For AMT23 oligotrophic surface waters, nitrate was mostly ±0.02 mmol m^{-3} and *Prochlorococcus* generally accounted for a higher proportion of TChla (Fig. 10). The competitive dominance of *Prochlorococcus* seems to be related to the ability to utilize ammonium more efficiently than *Synechococcus* (Moore et al., 2002), and also dissolved amino acids as demonstrated by Zubkov et al. (2003) in the oligotrophic and mesotrophic Arabian Sea.

The trophic conditions influencing phytoplankton during the cruises are therefore interesting to contemplate. While the AMT22 passage tracked more towards the centre of the N Atlantic gyre, the AMT23 track passed closer to the eastern boundary. Bigger differences between surface *Prochlorococcus* and *Synechococcus* proportions would therefore have been expected in the N Atlantic considering the difference between cruise tracks. In the S Atlantic, smaller differences were expected as the passages followed a similar course through the middle of the gyre. These expectations are similar to Zubkov et al. (1998), Heywood et al. (2006), Tarran et al. (2006) and Bracher et al. (2020) who observed greater abundance of *Prochlorococcus* in the mid-ocean gyres, while *Synechococcus* tended to be more numerically dominant near the boundaries of these systems where conditions change from oligotrophic to more mesotrophic. But the results in this study are contrary to the expectations and these previous observations as the data indicate that the differences between *Prochlorococcus* and *Synechococcus* proportions were consistent across the entire Atlantic transects (Fig. 5). This suggests some different responses to larger scale forcing affecting the whole basin during 2012 and 2013.

Strong water column stratification usually favours *Prochlorococcus* and previous studies have shown direct relationships between *Prochlorococcus* and water column stability (Bouman et al., 2011). Such

Table 4
Linear regression analysis between stratification and phytoplankton group proportions. Grey shading indicates significant relationships ($p < 0.05$). Diat-diatoms; Dino-dinoflagellates; Hapt-haptophytes; Pela-pelagophytes; Cryp-cryptophytes; Pras-prasinophytes; Syne-Synechococcus; Proc-Prochlorococcus.

	Group Proportion	Regression equation	R^2	F statistic	p value
AMT22 Surface					
Stratification index	**Diat**	y = -2.379x + 7.061	0.293	7.863	0.011
	Dino	y = -1.809x + 6.581	0.241	6.028	0.024
	Hapt	y = -6.217x + 30.915	0.336	9.612	0.006
	Pela	y = -4.356x + 14.935	0.435	14.603	0.001
	Cryp	y = -0.798x + 3.739	0.318	8.877	0.008
	Pras	y = -1.709x + 15.701	0.235	5.846	0.026
	Syne	y = 8.512x + 14.210	0.547	22.934	<0.001
	Proc	y = 8.756x + 6.859	0.543	22.600	<0.001
AMT23 Surface					
Stratification index	**Diat**	y = -2.771x + 10.171	0.142	7.104	0.011
	Dino	y = -0.940x + 6.411	0.149	7.542	0.009
	Hapt	y = -2.408x + 18.280	0.163	8.357	0.006
	Pela	y = -1.582x + 9.227	0.326	20.784	<0.001
	Cryp	y = -0.868x + 6.008	0.189	10.030	0.003
	Pras	y = -3.616x + 18.568	0.421	31.282	<0.001
	Syne	y = 5.439x + 11.792	0.516	45.761	<0.001
	Proc	y = 6.746x + 19.543	0.298	18.271	<0.001
AMT22 DCM					
Stratification index	**Diat**	y = -1.138x + 5.074	0.053	3.557	0.064
	Dino	y = -0.999x + 6.056	0.071	4.878	0.031
	Hapt	y = 2.014x + 28.522	0.109	7.827	0.007
	Pela	y = -0.153x + 11.549	0.001	0.061	0.806
	Cryp	y = 0.440x + 5.542	0.019	1.212	0.275
	Pras	y = -1.278x + 9.599	0.045	3.010	0.088
	Syne	y = -1.567x + 7.867	0.141	10.470	0.002
	Proc	y = 2.681x + 25.791	0.038	2.543	0.116
AMT23 DCM					
Stratification index	**Diat**	y = -1.176x + 3.890	0.108	6.324	0.015
	Dino	y = -0.384x + 3.349	0.020	1.070	0.306
	Hapt	y = -1.142x + 24.826	0.059	3.270	0.076
	Pela	y = -0.224x + 10.366	0.012	0.625	0.433
	Cryp	y = -0.727x + 8.290	0.098	5.630	0.021
	Pras	y = -0.902x + 13.083	0.026	1.366	0.248
	Syne	y = 2.233x + 16.327	0.152	9.329	0.004
	Proc	y = 2.323x + 19.870	0.071	3.949	0.052

clear direct and consistent relationships were not observed for our study. North of 30°N in the N Atlantic, and south of 30°S in the S Atlantic, stratification was similarly weaker compared to the equatorial regions during the two cruises. In the S Atlantic, this weak stratification coincided with the generally elevated surface *Synechococcus* proportions during both cruises, but in the N Atlantic, *Prochlorococcus* was substantially more dominant at the surface during AMT23 (Figs. 4 and 5). Between 0 and 30°N, much stronger stratification was observed during AMT22 (Fig. 4), and while we expected *Prochlorococcus* proportions to be higher, instead *Synechococcus* dominated at the surface (Fig. 5). In the S Atlantic, between 0 and 30°S, the opposite pattern was observed, with substantially stronger stratification during AMT23 with clear dominance of surface *Prochlorococcus* compared to AMT22, where stratification in this region was much weaker, with roughly equal *Prochlorococcus* and *Synechococcus* proportions (Figs. 4 and 5). Statistically significant, moderately strong positive correlations (Table 4) showed that stronger stratification favoured both *Prochlorococcus* and *Synechococcus* during AMT22 and AMT23.

The lack of clear consistent relationships between *Prochlorococcus* proportions and stratification in our study likely stem from the differences in the various physical processes that influence stratification, and these also likely explain the discrepancies observed between UML depth and the stratification index. While the seasonal coupling between atmospheric heating and ocean surface warming increases stratification and stabilises the upper mixed layer during spring and summer, the reverse happens during autumn and winter when stratification is reduced and deeper mixing takes place (Li et al., 2020; Mahadevan et al., 2016). However, changes in stratification may also result from variations in precipitation or evaporation, which would cause the surface layers to become either fresher or saltier, hence influencing density and water column stability. This is evident in that the stratification patterns (Fig. 4) were mirrored by changes in salinity along the transects (Figs. 2 and 3). Variations in wind forcing, horizontal advection of remotely formed water masses into our region of interest, and mesoscale variability (such as eddies and fronts) can also result in large-scale, regional or more localised changes in the water column stratification (Behrenfeld et al., 2006, Li et al., 2020; Mahadevan et al., 2016). In response to the simultaneous influence of these myriad of processes at various space and time scales, UML depth and stratification do not always co-vary.

At the DCM, there was a much higher proportion of *Prochlorococcus* and low *Synechococcus* along the whole transect on AMT22 (Fig. 6). AMT23 displayed an overall lower proportion of *Prochlorococcus* than

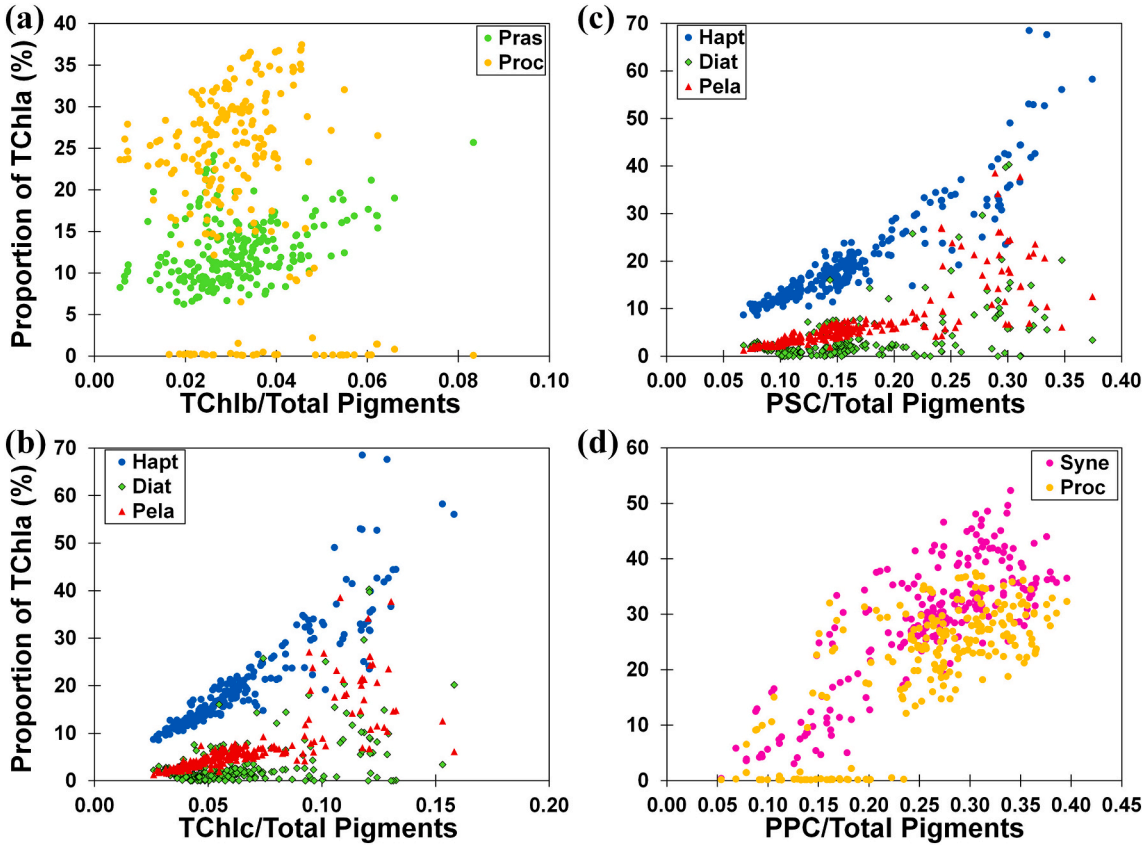

Fig. 8. Relationships between surface photo-pigment indices and selected phytoplankton group proportions for AMT22. TChlb = total chlorophyll *b*; TChlc = total chlorophyll *c*; PSC = photosynthetic carotenoids; PPC = photoprotective carotenoids. Pras-prasinophytetes Proc-*Prochlorococcus*; Hapt-haptophytes; Diat-diatoms; Pela-pelagophytes; Syne-*Synechococcus*.

AMT22 and a much higher proportion of *Synechococcus*, but overall *Prochlorococcus* still exceeded *Synechococcus* (Fig. 6). There were no obvious differences in DCM depth between AMT22 and AMT23, but TChla was higher overall at the DCM on AMT23, suggesting that there were more nutrients available at the DCM on AMT23. The greater nutrient availability at the DCM on AMT23 (Fig. 3d) likely resulted from large-scale advection or wind driven upwelling processes which would uplift the nutricline along the eastern boundary of the North Atlantic. This is supported by the overall higher proportions of *Synechococcus* at the DCM on AMT23 relative to AMT22 (Fig. 6). Differences between *Prochlorococcus* and *Synechococcus* were more pronounced in the N Atlantic, maybe because passage was closer to the eastern boundary of the gyre, but there was also a distinction in the S Atlantic where there were similar cruise tracks through the centre of the gyre. As described above, large-scale differences in stratification and upper mixed layer depth between AMT23 and AMT22 would result from variations in circulation patterns and differences in wind forcing, with more wind inducing less stratification and deeper mixing and vice versa. In the North Atlantic, particularly north of 30°N, despite the similar stratification index values and the greater nutrient availability at the DCM, the overall shallower UML during AMT23 suggested that the surface layers were more stable than during AMT22 (Fig. 4c, d), thus favouring higher proportions of *Prochlorococcus* at the surface (Fig. 5). In contrast, during the AMT22 transit through the central part of the North Atlantic, the generally stronger vertical mixing suggested by the overall deeper UML (Fig. 4c) and more elevated NO3 at the surface (Fig. 10) was more favourable for *Synechococcus* (Fig. 5b). In the South Atlantic, stronger water column stability, inferred from the generally shallower UML (Fig. 4c, d), should have favoured larger proportions of *Prochlorococcus* during AMT22 compared to AMT23. However, CHEMTAX indicated that surface *Prochlorococcus* proportions during AMT23 were in fact greater than those during AMT22 (Fig. 5b, e). Despite the stronger mixing in the South Atlantic during AMT23, there was much less NO3 at the surface than during AMT22 (Fig. 10), which favoured *Prochlorococcus* more strongly than *Synechococcus*. This suggests that although stronger wind mixing resulted in a deeper UML during AMT23, the overall nutrient supply to the surface layers may have been reduced by the existence of deeper nutriclines, as suggested by the overall higher stratification index values. During AMT22, nutriclines may have been much shallower, as suggested by the smaller stratification index values, which means that much less wind-induced vertical mixing would have been required to erode the nutricline and enhance nutrient supply to the surface layers. Such observations are in agreement with previous studies that demonstrated clear correlations between wind speeds and net community production (Ford et al., 2021), as well as UML, nutricline depth, and chlorophyll variability in the S Atlantic (Signorine et al., 2015).

The light environment also has an important role since light is required for photosynthesis and the creation of new biomass, and Letelier et al. (2004) and Cullen (2015) have discussed the required balance between the flux of nutrients and the light energy available for the growth of phytoplankton. Aiken et al. (2017) state that the Atlantic gyres are two-layer systems, where the surface layer has high light availability but is nitrogen limited, while the DCM is relatively nutrient replete but light limited. Seasonal observations indicate that while highest surface TChla occurs in winter, the maximum TChla at the DCM occurs in summer, all regulated by the seasonal change in solar insolation (Aiken et al., 2017). The light environment at the DCM during AMT22 and AMT23 can be inferred from the depth of the DCM and the depth of Zeu (Fig. 4c, d). North of 30°N, south of 30°S, and in the equatorial region roughly between 20°N and 20°S, the DCM was located

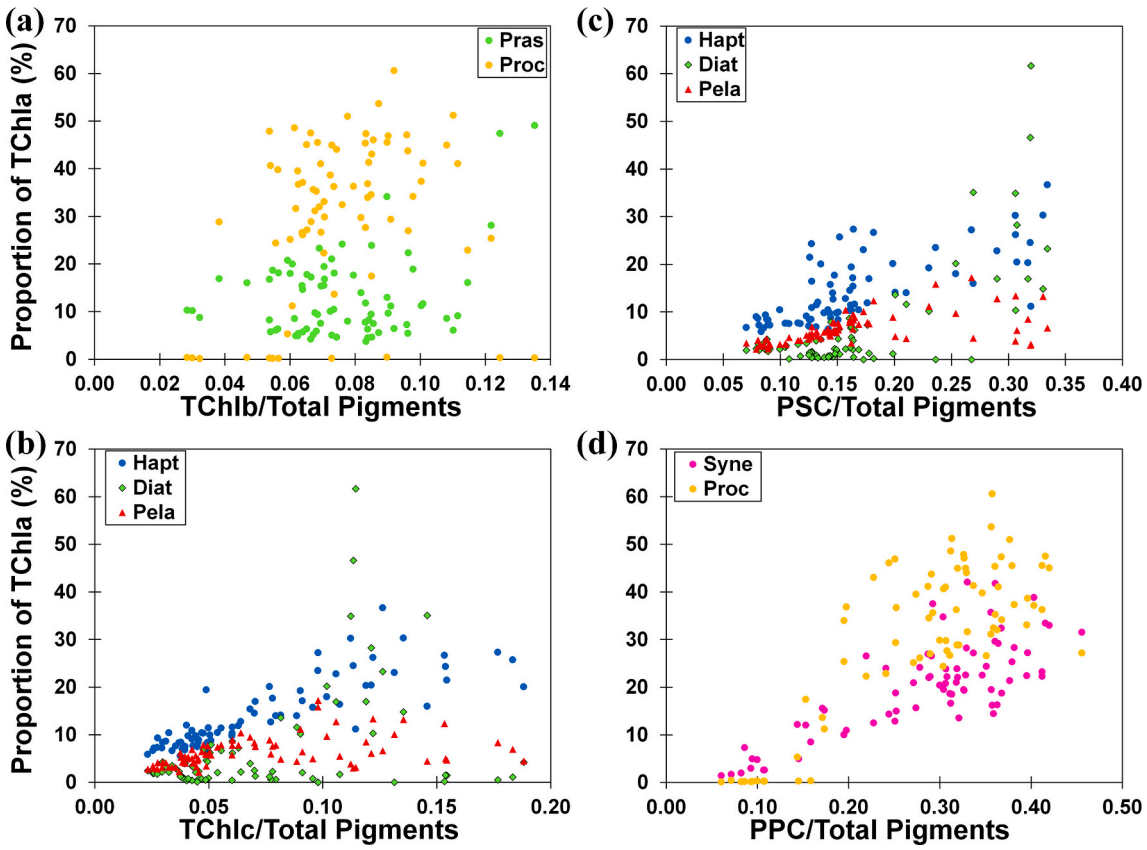

Fig. 9. Relationships between surface photo-pigment indices and selected phytoplankton group proportions for AMT23. TChlb = total chlorophyll *b*; TChlc = total chlorophyll *c*; PSC = photosynthetic carotenoids; PPC = photoprotective carotenoids. Pras-prasinophytetes Proc-*Prochlorococcus*; Hapt-haptophytes; Diat-diatoms; Pela-pelagophytes; Syne-*Synechococcus*.

within or at the base of the euphotic zone. Here the DCM phytoplankton would be receiving comparatively more light. Between 20 and 30°S and 20–30°N, the DCM was somewhat deeper than Zeu, where the DCM phytoplankton would be receiving comparatively less light. This same pattern is evident for both cruises. However, these differences were not large enough to be statistically significant, and thus we conclude that the DCM is essentially located at the base of the euphotic zone, where by definition there is 1% of the surface light available, indicating light limitation.

The ecological success of *Prochlorococcus* appears to be due to various unique characteristics. The cells have a particularly high surface area to volume ratio (Raven et al., 2005) and their evolution produced a very small cell size enabling them to compete more successfully in conditions of severe nutrient limitation (Dufresne et al., 2005). The average cell size for *Prochlorococcus* is 0.6 μm and *Synechococcus* is 0.9 μm. (Morel et al., 1993). Two distinct ecotypes evolved, one adapted to high light and the other to low light. Molecular studies revealed that high-light ecotypes contain the smallest genomes and dominate where there is strong stratification, while low-light eco-types have larger genomes and tend to be more prevalent under conditions of vertical mixing (Bouman et al., 2011). Low-light ecotypes are also larger as cell size is usually positively correlated with genome size (Connolly et al., 2008). The high-light strains of *Prochlorococcus* cannot utilize nitrate and nitrite (Moore et al., 2002) as they do not contain the appropriate assimilation genes and appear to survive in oligotrophic surface waters by utilizing ammonium (Rocap et al., 2003) and amino acids (Zubkov et al., 2003). Both *Prochlorococcus* ecotypes contain divinyl chlorophylls *a* and *b* thus enabling blue wavelength absorption (Moore et al., 1995) and therefore low-light strains can adapt well at depth to the change in spectrum and low irradiance. Furthermore, the low-light ecotype has nitrite reductase which is conducive to using nitrite as a nitrogen source but not nitrate (Rocap et al., 2003). Some strains contain a high proportion of divinyl chlorophyll *b* enabling greater absorption of low intensity blue light and this confers an advantage for survival at depth near the base of the euphotic zone (Moore et al., 1995). Due to its minute size, *Prochlorococcus* has a particularly high absorption efficiency, a high pigment content per cell, but a low light scattering efficiency (Morel et al., 1993), enhancing the probability of photons being absorbed instead of being scattered. All other phytoplankton types are more efficient at scattering than absorbing light (Morel et al., 1993). These advances in microbial molecular biology, physiology and bio-optical knowledge, highlights the adaptability of *Prochlorococcus* to dominate oligotrophic surface waters and also contribute substantially to communities deeper in the euphotic zone.

In summary, CHEMTAX analysis of AMT pigment data indicated that *Synechococcus* tended to be more dominant at the surface in the oligotrophic subtropical gyres and tropical regions in October–November 2012, while *Prochlorococcus* was dominant during the same seasons in 2013 when inorganic nitrate concentrations were extremely low. The communities at the DCM consisted primarily of *Prochlorococcus* and haptophytes in 2012, and *Prochlorococcus, Synechococcus* and haptophytes in 2013. Populations in the temperate northern and southern high latitudes were composed mostly of haptophytes, but also contributions by diatoms and dinoflagellates, pelagophytes and prasinophytes. The spring blooms in the temperate regions appear to be dominated by haptophytes (Egge et al., 2015). Photo-pigment indices indicated that TChla, consisting of monovinyl plus divinyl chlorophyll *a*, dominated the pigment pool, but PPCs were elevated at the surface being associated with the high proportions of *Prochlorococcus* and *Synechococcus*. PPCs were low at the DCM where there were increased proportions of PSC and TChlb. This investigation is a contribution to continuing investigations in the Atlantic Ocean towards improved

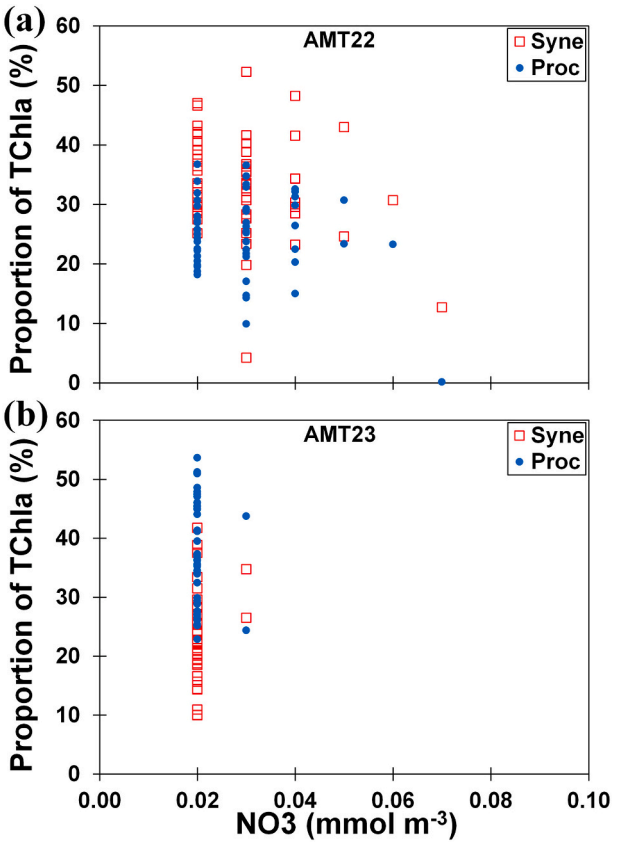

Fig. 10. Relationships between *Synechococcus* (Syne) and *Prochlorococcus* (Proc) group proportions and nitrate concentrations for the AMT22 surface between 47.88°N and 38.91°S, and the AMT23 surface between 46.62°N and 26.92°S.

understanding of the variability in phytoplankton across hydrographic gradients, important for predicting the adaptation of ocean ecosystems to global climate change.

Declaration of Competing Interest

The authors declare that they have no known competing financial interests or personal relationships that could have appeared to influence the work reported in this paper.

Data availability

The data that has been used is confidential.

Acknowledgements

We sincerely thank the officers and crews of the RRS *James Cook* and the RRS *James Clark Ross* for their skilled co-operation and assistance during the AMT cruises; L Pollard and G Dall'Olmo for cruise sampling on AMT22; D Cummings for pigment analysis; A Bargery and R Wright (British Oceanographic Data Centre) for hydrographic data. RB, TL and JV were supported by the South African National Research Foundation and Department of Forestry, Fisheries and Environment, and the Bayworld Centre for Research and Education. The Atlantic Meridional Transect is funded by the UK Natural Environment Research Council through its National Capability Long-term Single Centre Science Programme, Climate Linked Atlantic Sector Science (grant number NE/R015953/1). This study contributes to the international IMBeR project and is contribution number 370 of the AMT programme.

Appendix A. Supplementary data

Supplementary data to this article can be found online at https://doi.org/10.1016/j.jmarsys.2022.103844.

References

Agirbas, E., Martinez-Vicente, V., Brewin, R., Racault, M.-F., Airs, R., Llewellyn, C., 2015. Temporal changes in total and size-fractioned chlorophyll-a in surface waters of three provinces in the Atlantic Ocean (September to November) between 2003 and 2010. J. Mar. Syst. 150, 56–65.

Aiken, J., Rees, N., Hooker, S., Holligan, P., Bale, A., Robins, D., Moore, G., Harris, R., Pilgrim, D., 2000. The Atlantic meridional transect: overview and synthesis of data. Prog. Oceanogr. 45, 257–312.

Aiken, J., Pradhan, Y., Barlow, R., Lavender, S., Poulton, A., Holligan, P., Hardman-Mountford, N., 2009. Phytoplankton pigments and functional types in the Atlantic Ocean: a decadal assessment, 1995–2005. Deep-Sea Res. II 56, 899–917.

Aiken, J., Brewin, R., Dufois, F., Polimene, L., Hardman-Mountford, N., Jackson, T., Loveday, B., Hoya, S., Dall'Olmo, G., Stephens, J., Hirata, T., 2017. A synthesis of the environmental response of the North and South Atlantic Sub-Tropical Gyres during two decades of AMT. Prog. Oceanogr. 158, 236–254.

Barlow, R., Aiken, J., Holligan, P., Cummings, D., Maritorena, S., Hooker, S., 2002. Phytoplankton pigment and absorption characteristics along meridional transects in the Atlantic Ocean. Deep-Sea Res. I 49, 637–660.

Barlow, R., Aiken, J., Moore, G., Holligan, P., Lavender, S., 2004. Pigment adaptations in surface phytoplankton along the eastern boundary of the Atlantic Ocean. Mar. Ecol. Prog. Ser. 281, 13–26.

Barlow, R., Lamont, T., Kyewalyanga, M., Sessions, H., Morris, T., 2010. Phytoplankton production and physiological adaptation on the southeastern shelf of the Agulhas ecosystem. Cont. Shelf Res. 30, 1472–1486.

Barlow, R., Gibberd, M.-J., Lamont, T., Aiken, J., Holligan, P., 2016. Chemotaxonomic phytoplankton patterns on the eastern boundary of the Atlantic Ocean. Deep-Sea Res. I 111, 73–78.

Behrenfeld, M.J., O'Malley, R.T., Siegel, D.A., McClain, C.R., Sarmiento, J.L., Feldman, G.C., Milligan, A.J., Falkowski, P.G., Letelier, R.M., Boss, E.S., 2006. Climate-driven trends in contemporary ocean productivity. Nature 444, 752–755.

Bouman, H., Ulloa, O., Barlow, R., Li, W., Platt, T., Zwirglmaier, K., Scanlan, D., Sathyendranath, S., 2011. Water-column stratification governs the community structure of subtropical marine picophytoplankton. Environ. Microbiol. Rep. 3, 473–482.

Bracher, A., Xi, H., Dinter, T., Mangin, A., Strass, V., von Appen, W.-J., Wiegmann, S., 2020. High resolution water column phytoplankton composition across the Atlantic Ocean from ship-towed vertical undulating radiometry. Front. Mar. Sci. 7, 235.

Brewin, R.J.W., Hirata, T., Hardman-Mountford, N.J., Lavender, S.J., Sathyendranath, S., Barlow, R., 2012. The influence of the Indian Ocean dipole on interannual variations in phytoplankton size structure as revealed by earth observation. Deep-Sea Res. II 77-80, 117–127.

Brunet, C., Johnsen, G., Lavaud, J., Roy, S., 2011. Pigments and photoacclimation processes. In: Roy, S., Llewellyn, C., Egeland, E., Johnsen, G. (Eds.), Phytoplankton Pigments: Characterization, Chemotaxonomy and Applications in Oceanography. Cambridge University Press, Cambridge, pp. 445–471.

Connolly, J., Oliver, M., Beaulieu, J., Knight, C., Tomanek, L., Moline, M., 2008. Correlated evolution of genome size and cell volume in diatoms (Bacillariophyceae). J. Phycol. 44, 124–131.

Cullen, J., 2015. Subsurface chlorophyll maximum layers: enduring enigma or mystery solved? Annu. Rev. Mar. Sci. 7 (207), 239.

Dufresne, A., Garczarek, L., Partensky, F., 2005. Accelerated evolution associated with genome reduction in a free-living prokaryote. Genome Biol. 6, R14.

Egge, J., Aksnes, D., 1992. Silicate as regulating nutrient in phytoplankton competition. Mar. Ecol. Prog. Ser. 83, 281–289.

Egge, E., Johannessen, T., Andersen, T., Eikrem, W., Bittner, L., Larsen, A., Sandaa, R., Edvardsen, B., 2015. Seasonal diversity and dynamics of haptophytes in the Skagerrak, Norway, explored by high-throughput sequencing. Mol. Ecol. 24, 3026–3042.

Field, C., Behrenfeld, M., Randerson, J., Falkowski, P., 1998. Primary production of the biosphere: integrating terrestrial and oceanic components. Science 281, 237–240.

Ford, D., Tilstone, G., Shutler, J., Kitidis, V., Lobanova, P., Schwarz, J., Poulton, A., Serret, P., Lamont, T., Chuqui, M., Barlow, R., Lozano, J., Kampel, M., Brandini, F., 2021. Wind speed and mesoscale features drive net autotrophy in the South Atlantic Ocean. Remote Sens. Environ. 260, 112435.

Garzoli, S.L., Garraffo, Z., 1989. Transports, frontal motions and eddies at the Brazil-Malvinas currents confluence. Deep-Sea Res. 36, 681–703.

Gibb, S., Barlow, R., Cummings, D., Rees, N., Trees, C., Holligan, P., Suggett, D., 2000. Surface phytoplankton pigment distributions in the Atlantic Ocean: an assessment of basin scale variability between 50°N and 50°S. Prog. Oceanogr. 45, 339–368.

Heywood, J., Zubkov, M., Tarran, G., Fuchs, B., Holligan, P., 2006. Prokaryote plankton standing stocks in oligotrophic gyres and equatorial provinces of the Atlantic Ocean: evaluation of inter-annual variability. Deep-Sea Res. II 53, 1530–1547.

Higgins, H., Wright, S., Schluter, L., 2011. Quantitative interpretation of chemotaxonomic pigment data. In: Roy, S., Llewellyn, C., Egeland, E., Johnsen, G. (Eds.), Phytoplankton Pigments: Characterization, Chemotaxonomy and Applications in Oceanography. Cambridge University Press, Cambridge, pp. 257–313.

Jeffrey, S., Wright, S., Zapata, M., 2011. Microalgal classes and their signature pigments. In: Roy, S., Llewellyn, C., Egeland, E., Johnsen, G. (Eds.), Phytoplankton Pigments: Characterization, Chemotaxonomy and Applications in Oceanography. Cambridge University Press, Cambridge, pp. 3–77.

Johnsen, G., Bricaud, A., Nelson, N., Prezelin, B., Bidigare, R., 2011. In vivo bio-optical properties of phytoplankton pigments. In: Roy, S., Llewellyn, C., Egeland, E., Johnsen, G. (Eds.), Phytoplankton Pigments: Characterization, Chemotaxonomy and Applications in Oceanography. Cambridge University Press, Cambridge, pp. 496–537.

Letelier, R., Karl, D., Abbott, M., Bidigare, R., 2004. Light driven seasonal patterns of chlorophyll and nitrate in the lower euphotic zone of the North Pacific subtropical gyre. Limnol. Oceanogr. 49, 508–519.

Li, G., Cheng, L., Zhu, J., Trenberth, K.E., Mann, M.E., Abraham, J.P., 2020. Increasing ocean stratification over the past half-century. Nat. Clim. Chang. 10, 1116–1123.

Mackey, M., Mackey, D., Higgins, H., Wright, S., 1996. CHEMTAX- a program for estimating class abundances from chemical markers: application to HPLC measurements of phytoplankton. Mar. Ecol. Prog. Ser. 144, 265–283.

Mahadevan, A., D'Asaro, E., Lee, C., Perry, M.J., 2012. Eddy-driven stratification initiates North Atlantic spring phytoplankton blooms. Science 337, 54–58.

Maloney, C., Field, J., 1991. The size-based dynamics of plankton food webs. I. a simulation model of carbon and nitrogen flows. J. Plankton Res. 13, 1003–1038.

Mitchell, G., Brody, E., Holm-Hansen, O., McClain, C., Bishop, J., 1991. Light limitation of phytoplankton biomass and macronutrient utilization in the Southern Ocean. Limnol. Oceanogr. 36, 1662–1677.

Moore, L., Goericke, R., Chisholm, S., 1995. Comparative physiology of *Synechococcus* and *Prochlorococcus*: influence of light and temperature on growth, pigments, fluorescence and absorptive properties. Mar. Ecol. Prog. Ser. 116, 259–275.

Moore, L., Post, A., Rocap, G., Chisholm, S., 2002. Utilization of different nitrogen sources by the marine cyanobacteria *Prochlorococcus* and *Synechococcus*. Limnol. Oceanogr. 47, 989–996.

Morel, A., 1988. Optical modelling of the upper ocean in relation to its biogenous matter content (case 1 waters). J. Geophys. Res. 93, 10749–10768.

Morel, A., Ahn, Y.-H., Partensky, F., Vaulot, D., Claustre, H., 1993. *Prochlorococcus* and *Synechococcus*: a comparative study of their optical properties in relation to their size and pigmentation. J. Mar. Res. 51, 617–649.

Nunes, S., Perez, G., Latasa, M., Zamanillo, M., Delgado, M., Ortega-Retuerta, E., Marrasé, C., Simó, R., Estrada, M., 2019. Size fractionation, chemotaxonomic groups and bio-optical properties of phytoplankton along a transect from the Mediterranean Sea to the SW Atlantic Ocean. Sci. Mar. 83, 87–109.

Partensky, F., Hess, W., Vaulot, D., 1999. Prochlorococcus, a marine photosynthetic prokaryote of global significance. Microbiol. Mol. Biol. Rev. 63, 106–127.

Platt, T., Sathyendranath, S., 2008. Ecological indicators for the pelagic zone of the ocean from remote sensing. Remote Sens. Environ. 112, 3426–3436.

Poulton, A., Holligan, P., Hickman, A., Kim, Y.-N., Adey, T., Stinchcombe, M., Holeton, C., Root, S., Woodward, E., 2006. Phytoplankton carbon fixation, chlorophyll biomass and diagnostic pigments in the Atlantic Ocean. Deep-Sea Res. II 53, 1593–1610.

Poulton, A., Holligan, P., Charalampopoulou, A., Adey, T., 2017. Coccolithophore ecology in the tropical and subtropical Atlantic Ocean: new perspectives from the Atlantic meridional transect (AMT) programme. Prog. Oceanogr. 158, 150–170.

Raven, J., Finkel, Z., Irwin, A., 2005. Picophytoplankton: bottom-up and top-down controls on ecology and evolution. Vie et Milieu 55, 209–215.

Rees, A., Nightingale, P., Poulton, A., Smyth, T., Tarran, G., Tilstone, G., 2017. The Atlantic Meridional Transect programme (1995–2016). Prog. Oceanogr. 158, 3–18.

Robinson, C., Poulton, A., Holligan, P., Baker, A., Forster, G., Gist, N., Jickells, T., Malin, G., Upstill-Goddard, R., Williams, R., Woodward, M., Zubkov, M., 2006. The Atlantic Meridional Transect (AMT) programme: a contextual view 1995–2005. Deep-Sea Res. II 53, 1485–1515.

Rocap, G., Larimer, F., Lamerdin, J., Malfatti, S., Chain, P., Ahlgren, N., et al., 2003. Genome divergence in two *Prochlorococcus* ecotypes reflects oceanic niche differentiation. Nature 424, 1042–1047.

Signorine, S., Franz, B., McClain, C., 2015. Chlorophyll variability in the oligotrophic gyres: mechanisms, seasonality and trends. Front. Mar. Sci. 2, 1.

Smyth, T., Quartly, G., Jackson, T., Tarran, G., Woodward, M., Harris, C., Gallienne, C., Thomas, R., Airs, R., Cummings, D., Brewin, R., Kitidis, V., Stephens, J., Zubkov, M., Rees, A., 2017. Determining Atlantic Ocean province contrasts and variations. Prog. Oceanogr. 158, 19–40.

Tarran, G., Heywood, J., Zubkov, M., 2006. Latitudinal changes in the standing stocks of nano-and picoeukaryotic phytoplankton in the Atlantic Ocean. Deep-Sea Res. II 53, 1516–1529.

Thomson, R., Fine, I., 2003. Estimating mixed layer depth from oceanic profile data. J. Atmos. Ocean. Technol. 20, 319–329.

Tilstone, G., Lange, P., Misra, A., Brewin, R., Cain, T., 2017. Micro-phytoplankton photosynthesis, primary production and potential export production in the Atlantic Ocean. Prog. Oceanogr. 158, 109–129.

Van Heukelem, L., Hooker, S., 2011. The importance of a quality assurance plan for method validation and minimizing uncertainties in the HPLC analysis of phytoplankton pigments. In: Roy, S., Llewellyn, C., Egeland, E., Johnsen, G. (Eds.), Phytoplankton Pigments: Characterization, Chemotaxonomy and Applications in Oceanography. Cambridge University Press, Cambridge, pp. 195–242.

Woodward, E., Rees, A., 2001. Nutrient distributions in an anticyclonic eddy in the North East Atlantic Ocean, with reference to nanomolar ammonium concentrations. Deep-Sea Res. II 48, 775–794.

Wright, S., 2008. Chemtax version 1.95 for calculating the taxonomic composition of phytoplankton populations. https://doi.org/10.4225/15/59fff1c5ea8fc.

Wright, S., Ishikawa, A., Marchant, H., Davidson, A., van den Enden, R., Nash, G., 2009. Composition and significance of picophytoplankton in Antarctic waters. Polar Biol. 797–808.

Zapata, M., Rodríguez, F., Garrido, J., 2000. Separation of chlorophylls and carotenoids from marine phytoplankton: a new HPLC method using a reversed phase C8 column and pyridine containing mobile phases. Mar. Ecol. Prog. Ser. 195, 29–45.

Zubkov, M., Sleigh, M., Tarran, G., Burkill, P., Leakey, R., 1998. Picoplankton community structure on an Atlantic transect from 50°N to 50°S. Deep-Sea Res. I 45, 1339–1355.

Zubkov, M., Sleigh, M., Burkill, P., Leakey, R., 2000. Picoplankton community structure on the Atlantic Meridional Transect: a comparison between seasons. Prog. Oceanogr. 45, 369–386.

Zubkov, M., Fuchs, B., Tarran, G., Burkill, P., Amann, R., 2003. High rate of uptake of organic nitrogen compounds by *Prochlorococcus* cyanobacteria as a key to their dominance in oligotrophic oceanic waters. Appl. Environ. Microbiol. 69, 1299–1304.